Eurographics Workshop on Visual Computing for Biology and Medicine (2016)
S. Bruckner, B. Preim, and A. Vilanova (Editors)

Coherence Maps for Blood Flow Exploration

Rickard Englund[1] , Timo Ropinski[2] and Ingrid Hotz[1]

[1]Interactive Visualization Group, Linköping University, Sweden
[2]Visual Computing Group, Ulm University, Germany

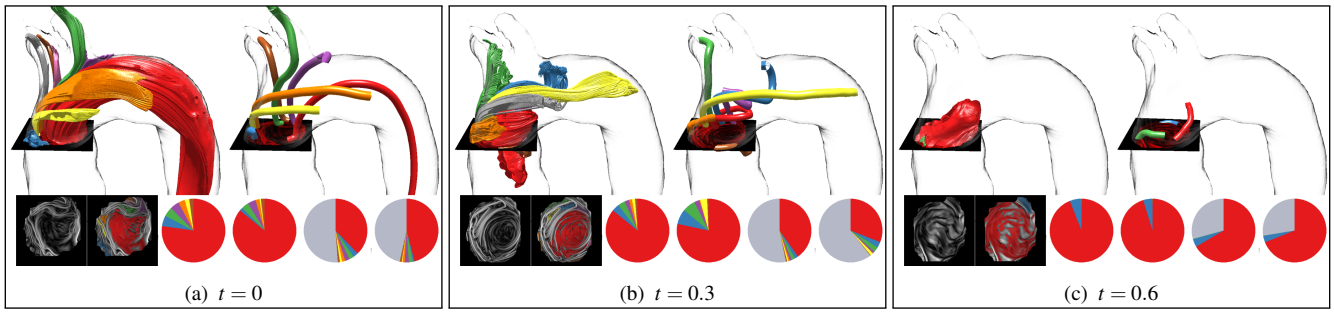

(a) $t = 0$ (b) $t = 0.3$ (c) $t = 0.6$

Figure 1: The results from applying the techniques described in the paper on a 4D flow MRI scan of a heart to 3 different timesteps t. For each timestep we see all pathlines from the seven most prominent clusters on the top left (except for $t = 0.6$ where only 3 clusters were found) and on the top right we see the representatives for these clusters. On the bottom row we first see the coherence map followed by the map with the located region marked by their representative color. The first and third pie chart show the size of the cluster in terms of pathline count and the second and fourth show the size in terms of rate of flow through the slice at the initial timestep. The third and fourth pie chart also include non-coherent flow into the visualization represented by the gray slice.

Abstract

Blood flow data from direct measurements (4D flow MRI) or numerical simulations opens new possibilities for the understanding of the development of cardiac diseases. However, before this new data can be used in clinical studies or for diagnosis, it is important to develop a notion of the characteristics of typical flow structures. To support this process we developed a novel blood flow clustering and exploration method. The method builds on the concept of coherent flow structures. Coherence maps for cross-sectional slices are defined to show the overall degree of coherence of the flow. In coherent regions the method summarizes the dominant blood flow using a small number of pathline representatives. In contrast to other clustering approaches the clustering is restricted to coherent regions and pathlines with low coherence values, which are not suitable for clustering and thus are not forced into clusters. The coherence map is based on the Finite-time Lyapunov Exponent (FTLE). It is created on selected planes in the inflow respective outflow area of a region of interest. The FTLE value measures the rate of separation of pathlines originating from this plane. Different to previous work using FTLE we do not focus on separating extremal lines but on local minima and regions of low FTLE intensities to extract coherent flow. The coherence map and the extracted clusters serve as basis for the flow exploration. The extracted clusters can be selected and inspected individually. Their flow rate and coherence provide a measure for their significance. Switching off clusters reduces the amount of occlusion and reveals the remaining part of the flow. The non-coherent regions can also be explored by interactive manual pathline seeding in the coherence map.

Categories and Subject Descriptors (according to ACM CCS): Computer Graphics [I.3.7]: Three-Dimensional Graphics and Realism—Color, shading, shadowing, and texture

1. Introduction

Blood flow analysis plays an increasing role in medical applications. Magnetic resonance imaging (MRI) has developed to be an important tool for diagnosis of cardiac diseases and besides providing morphological information it is now also possible to measure the blood flow directly. Also numerical simulations are used to understand the link between the blood flow and the functionality of the cardiovascular system or the severeness of aneurysms. With

DOI: 10.2312/vcbm.20161274

the development of these techniques the complexity of the resulting data sets is also increasing continuously. Appropriate analysis and visualization tools specifically target to blood flow analysis are required. Questions to be answered are related to the characterization, quantification and automatic extraction of relevant blood flow patterns from the data. When visualizing flow phenomena, often particle-based representations are exploited which depict flow features via integral curves. While such curves allow for an intuitive representation of flow, they come at the downside that the number of curves to be shown is limited. Several techniques have been developed with the goal to reduce the number of integral curves to deal with clutter and occlusion. Within these techniques, clustering-based techniques [OJCJP16, MJL*13] play an important role, as they summarize the flow behavior using a few cluster representatives based on an underlying similarity metric. While the resulting curve sets are useful in many cases, at least as many cases exist where the resulting cluster representatives do not meet the expectations of the investigating domain experts. In some cases, e.g., flows exhibiting turbulent behavior, clustering would also be in general inadequate to capture the entire flow. Furthermore, clustering-based approaches are mostly applied in a fully automatic pipeline and the clustering process itself is hidden from the user. This makes immediate verification of the clustering result and its quality very hard, whereas a clear understanding of the relevance of the clusters is essential for a proper flow analysis. Therefore, algorithms are required which allow for the generation of representative subsets that can be altered in an intuitive manner, and at the same time highlight regions where clustering is not possible.

In this paper, we present a novel algorithm, which generates easily adaptable representative curve subsets for blood flow data. The algorithm exploits the fact that blood flow has clearly defined inflow and outflow areas which are used to generate a two-dimensional summary plot of the flow behavior in terms of flow coherency [Hus83, SLM05]. We refer to these 2D planes as as *coherence maps*, which guide the automatic respective semi-automatic clustering and seeding process. Our basic assumption is that within coherent regions the flow can be well represented by one individual line while regions exhibiting a low degree of coherence have to be treated differently. Flow coherence provides an intuitive similarity measure that can be interpreted by both a computer, generating an initial clustering, and a human, who might want to adapt and understand the computed results. Technically we use the Finite-time Lyapunov Exponent (FTLE) [Hal01] which measures separation in the flow and thus is a valuable measure to distill coherent regions, which are characterized by low FTLE values. Compared to other frequently used similarity measures, this is a simplified but direct measure of entire curve coherence. While we will show how to use the coherence map to automatically generate clusters and extract representatives, we will also show how the computed coherence maps can be utilized as an intuitive user interface for adapting the set of coherent curves. By visually inspecting coherence maps it becomes easy to spot features in the flow, relate them to overlaid seed points, and adapt those seed points to generate an alternative curve subset. At the same time the coherence map conveys information about the size and coherence of the clustered regions and about the regions that cannot be well represented by clusters. Those regions can then be interactively explored by manual seeding. The contribution of the flow to the individual coherent regions is also displayed in pie charts which can be used to turn on and off the cluster visualization. They also give an impression of change of the flow coherence over a cardiac cycle. Our proposed FTLE-based algorithm can be used for both, to automatically generate a meaningful subset of integral curves, and second to adapt this subset intuitively to match the expectations of the user. Thus, the method provides a valuable tool for researchers in blood flow analysis to explore flow data with the goal to build an intuition and hypothesis about typical or atypical blood flow structures, which can build the basis for quantitative analysis in the clinical context in the future.

The remainder of this paper is structured as follows. We will first discuss work related to our approach in Section 2. Section 3 will then introduce the technical background considered when realizing the proposed algorithm. In Section 4 we introduce two FTLE analysis techniques, which are used to automatically compute seed points for a given vector field. The results achieved when applying the presented technique to real world data, are discussed in Section 5. Finally, the paper concludes in Section 6.

2. Related Work

Within this section, we will discuss the previous work and how it is related to our approach. We will first discuss concepts for integral curve filtering, before we describe relevant blood flow visualization techniques.

Integral curve filtering. Path and streamline visualizations are among the most intuitive and popular visualization techniques for 3D flow, and they are frequently applied in different areas, as for instance blood flow visualization. As the major challenge thereby is to deal with occlusion, various streamline placement algorithms have been developed to achieve a uniform coverage of the domain that is sparse but still captures the most important features of the field. While this works pretty well for 2D fields [MAD05, RPH*09], it is much more challenging for 3D flows. Here, importance controlled destiny fields or streamline measures are introduced to guide the seeding, which are in some cases combined with view-dependent criteria [MCHM10, GBWT11]. Popular importance criteria are based on entropy [LMSC11, CYY*11], or geometric descriptors of flow features. Günther et al. [GRT13] have applied view-dependent transparency to improve the perceptibility of large sets of streamlines. Another way to deal with the large amount of lines are filtering methods, which can be subsumed under the concept of predicates for path- or streamlines [SGSM08, BPM*13, KGP*13]. Clustering methods enable grouped regions of similar lines, which also results in a clearer image. Many methods use a pairwise comparison of the lines applying different similarity measures and streamline descriptors [MJL*13, YWSC12, LCL*13]. While in many cases the results of clustering algorithms are hard to predict, in the context of fiber visualization line clustering techniques have been evaluated by Moberts et al. [MVvW05]. Furthermore, an evaluation of different streamline clustering techniques for blood flow data has been published by Oeltze et. al. [OLTP12].

The approach proposed in this paper is most directly related to the concept of topological field segmentation, an idea that builds on the theory of dynamical systems. Such methods reduce the flow to a structural skeleton consisting of critical points and separating lines and surfaces. Vector field topology leads to a natural seg-

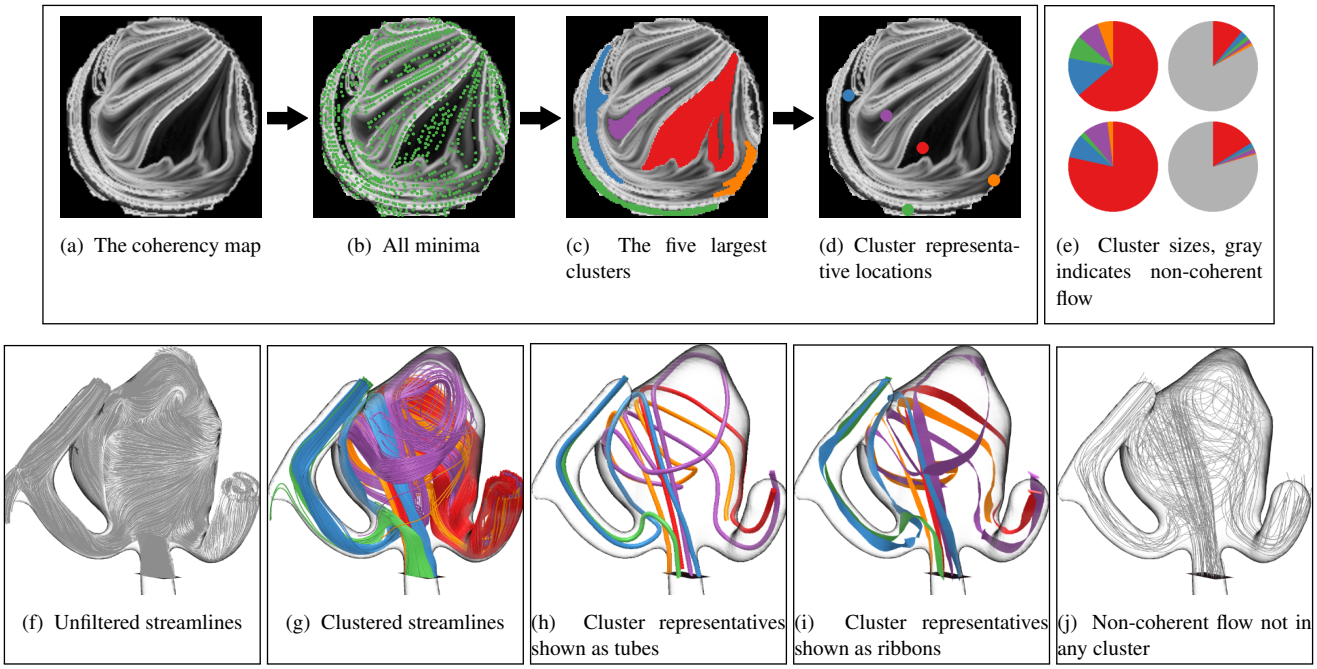

Figure 2: Visualization of blood flow simulated in an aneurysm. The top row shows the clustering pipeline, starting with the constructed coherence map (a), annotated with all the local minima (b) followed by the areas five most prominent clusters (c) and finally the location of the representatives(d). The size of the cluster is depicted charts in (e) with the pie where the size of the slices on the top row represent amount of streamlines in each cluster while on the bottom row the size represent the flow-rate. In the bottom row we show all sampled streamline (f) used for the calculation of the coherence map. (g) shows all streamlines of the five most prominent clusters. (h) and (i) display the representative of these clusters rendered as tubes and as ribbons respectively. (j) shows the pathlines that is located in non-coherent regions.

mentation of the domain in regions of similar streamline behavior. Recent work deals with efficient ways for simplification and tracking of topological structures [TSH01, GTS*04]. However, the use of topology in practical applications is still very limited due to the complexity of the results, especially for 3D data. A second limitations is its restriction to stationary fields. Among the several attempts to introduce variants appropriate for the topological investigation of time-dependent flows [Hal01, KRaHCH*16], the most popular concepts rely on the notion of coherent structures [Hus83, SLM05, KHH12], which is often associated with the Finite Time Lyapunov exponent (FTLE). After its introduction to the visualization community by Haller [Hal01], several variants have been developed [KPH*09, PPSS14] and much effort has been put into the development of efficient computation methods [GGTH07, SP07, BGT12] and the robust extraction of the separating ridges and surfaces [POS*11, LM10, FSP12]. Until now FTLE has been applied mostly to flow analysis in the context with mixing [Cha10, SCTC12]. Recently there have also been first attempts to extract separation structures for blood flow data [ST08, SAG10, KGG*12]. Similar, as for vector field topology, the most severe limitation is the complexity of the ridges that separate coherent regions from each other. For 3D data sets these are complex surfaces, for which not only the extraction is a challenging task but also the visualization of the results. This motivated us to focus on the coherent regions themselves instead of the separating structures and use distinguished 2D cross sections for the flow analysis which can be specified in a natural way for blood flow. Garth et al. [GGTH07] also computed FTLE on 2D cross sections to characterize the coherence of particles. In contrast to our approach they focus on high FTLE values within the slices. However, they also suggest that these images could be used for manual line seeding.

Blood flow visualization. Along with the development and improvement of imaging modalities to measure blood flow (4D flow MRI [MKE11]) and the availability of respective simulation data [Lan13] there is an increasing interest in flow visualization methods specifically tailored to blood flow analysis for medical diagnosis. Typical visualization methods used in the medical field are pathline visualizations in combination with different color codings and statistical measures [ECE*10, SPK*12]. However, the development of more advanced methods is an active field of research in visualization. A survey of such methods can be found in the report by Köhler et al. [KBvP*15]. Directly relevant to our approach is the work by Born et. al., who use predicates for semantic filtering of the pathlines [BPM*13], but also the application of illustrative visualization methods to provide a comprehensible context visualization [BMGS13], as well as the explicit extraction of flow features like vortices [CBB*14]. Gasteiger et al. [GNKP10, GNBP11] developed rendering methods to efficiently support the flow within the surrounding vessel morphology by combining illustrative rendering styles. In their follow-up work they developed automatic

methods to detect hemodynamic characteristics in aneurysms related to the inflow jet and its impingement zone [GLvP*12]. An novel approach to make flows comparable has been presented by Angelelli et al. [AH11]. They proposed to straighten the tubular flow in the aorta for a side-by-side visualization. Van Pelt et al. presented a technique for exploring blood flow by probing, whereby they combine illustrative rendering and vector clustering [vPBB*11, vPJtHRV12].

Since vortices are considered being a critical feature for blood flow they are also in the focus of some blood flow analysis methods. Köhler et al. [KGP*13] developed a semi-automatic vortex extraction method using line predicates for different vortex identifiers. Byrne et al. [BC13] used vector field topological methods for the extraction of vortices. Their ideas have been used and further improved by Oeltze et al. [OJCJP16] for an illustrative rendering of vortex structures in aneurysms. Further, van Pelt et al. [vPFCV14] use pattern matching methods to detect helical and vortical patterns, whereby the extracted patterns are used for a comprehensive visualization of the cardiovascular anatomy. In recent work Meuschke et al. proposed a semi-automatic vortex flow classification in the aorta [MKP*16].

3. Coherent Structures and the Finite-time Lyapunov Exponent

The central concept of the clustering and seeding methods developed in this work are coherent structures. Initially, these structures have been introduced as a concept referring to some orderly structures in the flow. While the concept stayed very vague for a long time a particular realization by Haller [Hal01] became popular over the last decade. He proposed to consider distinguished lines or surfaces in the flow field which can be considered to be material boundaries. Furthermore, he introduced a measure to detect such structures which is a finite variant of the Lyapunov exponent. In the following we briefly describe this measure and how it is applied within our context. The Lyapunov Exponent (LE) originates from the theory of dynamical systems. It is a metric for the separation rate of infinitesimally close trajectories as time approaches infinity. For flow fields with a bounded time range we can limit the observation time to a finite time interval, this allows us to use the Lyapunov Exponent as a measure of coherence in the flow field, the Finite-time Lyapunov Exponent (FTLE) . A high FTLE value indicates high separation (forward advection) or convergence (backward advection) of particles emitted at infinitesimal proximity. Haller states that the extremal structures of the FTLE field are possible boundaries of of Lagrangian coherent structures. In contrast, a low FTLE value indicates high coherence within a close neighborhood. This is the property which we use to extract coherent clusters form the flow.

The definition of FTLE uses the construct of a flow map $\phi_{t_0}^T$, which maps points at start positions x_0 at time t_0 to its advected position $x(T;t_0,x_0)$ after time T

$$\phi_{t_0}^T : x_0 \mapsto x(T;t_0,x_0) = \phi_{t_0}^T(x).$$

FTLE is then defined as the logarithm of the maximum relative stretching in direct analogy to the definition of the LE. Hereby, maximum stretching is represented by the maximum eigenvalue of

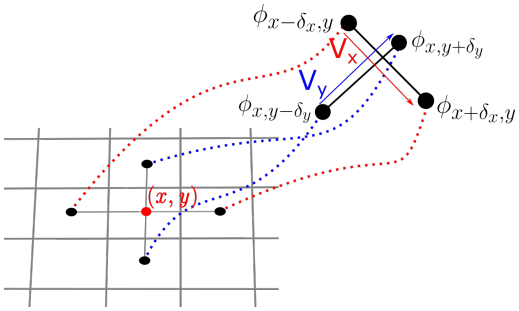

Figure 3: The calculation of the FTLE for grid point (x,y) is performed by using V_x and V_y to approximate the Jacobian matrix $J = [V_x \quad V_y]$.

the Cauchy-Green strain tensor $J^T J$, where $J = \nabla \phi_{t_0}^T$ is the Jacobian of the flow map.

$$FTLE = \frac{1}{t - t_0} ln \left| \lambda_{max} \left(J^T J \right) \right|, \tag{1}$$

where λ_{max} is the largest eigenvalue of $J^T J$. It is common to calculate the FTLE on a regular grid to approximate its real values. The flow map is computed for each grid cell, emitting and advecting a particle through the flow field and storing its final locations in the cell. The Jacobian of the flow map is then approximated using a finite differences method. A critical parameter for the FTLE computation is the time interval T which has to be chosen carefully. In general higher values of T result in more crisp structures. In the case of periodic flows, e.g., blood flow over one heart cycle, a good guiding value for T is the duration of one temporal period, which we will use in our examples accordingly.

We are especially interested in the FTLE values on two dimensional embedded planes. On the plane we emit particles in a regular grid at time t_0 and advect them through the flow field. The locations of the particles after advection builds the flow map $\phi_{t_0}^T$. The calculation of the FTLE for grid point (x,y) is illustrated in Figure 3. First we first compute the vectors V_x and V_y as

$$V_x = \frac{1}{2\delta_x} \left(\phi_{t_0}^T(x+\delta_x,y) - \phi_{t_0}^T(x-\delta_x,y) \right) \tag{2}$$

$$V_y = \frac{1}{2\delta_y} \left(\phi_{t_0}^T(x,y+\delta_y) - \phi_{t_0}^T(x,y-\delta_y) \right), \tag{3}$$

where $\phi_{(x,y)}$ is the location stored in the flow map for point (x,y) and δ_x and δ_y are the offset distance from grid point (x,y) to its nearest neighbor. Then V_x and V_y are used to approximate the Jacobian matrix $J = [V_x \quad V_y]$. The FTLE is finally calculated using Equation 1.

4. Coherent Flow Feature Extraction and Exploration

Our flow analysis method has been designed for flow data that has a clearly defined inflow and outflow area without internal sources. Such data typically results from blood flow simulations or measurements in a vessel system. The basic assumption is that all flow has to pass through the defined inflow and outflow areas and the investigation of all pathlines passing through these areas provides

a valuable summary of the flow structures in the entire volume. Therefore, our method distills flow features based on a close inspection of these summaries. Since FTLE values provide a solid measure for flow coherence we use FTLE as the basic underlying metric for automatic clustering and feature extraction and for manual exploration. The proposed feature extraction and analysis pipeline comprises the following parts:

(i) Generation of a two-dimensional coherence map (Sec. 4.1),
(ii) Automatic extraction of coherent regions (Sec. 4.2)
(iii) Coherent flow feature representation (Sec. 4.3)
(iv) Flow feature exploration (Sec. 4.4).

The individual steps will be explained in the following subsection.

4.1. Two-dimensional Coherence Maps

Instead of computing the FTLE values for the entire flow, we compute its values only on embedded planes. As planes we use a slice through the volume covering the inflow or outflow region of the flow, and thus capturing all pathlines entering or exiting the volume. The placement of the plane is done by the user in a 3D scene in which the plane is displayed together with a 3D rendering of the anatomy and additionally aided by displaying information derived from available volumetric data, such as velocity magnitude or anatomy, on 2D slices.. An example for the placement of such a plane for an aneurysm blood flow simulation can bee seen in Figure 2 (*bottom row*). When the plane has been placed at the desired location we construct the coherence map by calculating the FTLE values for each pixel in the map. This is done in a two step process. In the first step we trace a pathline for each pixel in the map, this is parallelized using OpenMP where each thread traces a set of pathlines. In the second step we calculate the FTLE value for each pixel by using the end positions of the 4 neighboring pathlines as described in section 3 and are parallelized in the manner as the first step. The resulting map exhibits the typical structures of FTLE showing ridges indicating a flow separation and enclosed connected regions, see Figure 2 (*a-e*). Pathlines within theses regions exhibit a very similar behavior within the flow volume and will build our coherent features. However, the coherence map also contains areas where the separating structures show a high spatial frequency and are not very crisp. We refer to these regions as 'non-coherent' regions, which cannot be assigned to any dominant flow feature and will be subject for an interactive exploration. These non-coherent areas of the flow are typically ignored in clustering algorithms and not represented by any cluster. Thus, the coherence map in itself already contains much valuable information for the exploration of flow. Garth et al. [GGTH07] also computed FTLE on manually defined 2D cross sections capturing the coherence of particles with application for general flow fields. However they focus on locations with high FTLE values within the slices.

4.2. Automatic Coherent Region Extraction

Commonly FTLE is used to extract material separation lines and surfaces from the flow, which correspond to the extremal structures of the FTLE field. In general these structures have a high complexity and their extraction is a challenge in itself and likewise is their visualization. Instead of considering these separating features we focus on the enclosed regions which exhibit a coherent flow behavior. To identify coherent regions we propose an algorithm that first cluster the local minima in the FTLE map and then performs a region growing to expand regions around the minima. Since we want to cluster regions of coherent flow we like to prevent inclusion regions with high FTLE values, therefore we introduce a coherence threshold that will be used in a few places through the algorithm. A pixel is classified as a minima and used for clustering if it has a lower FTLE value than its 8 nearest neighbors and if its FTLE value is less than the coherence threshold.

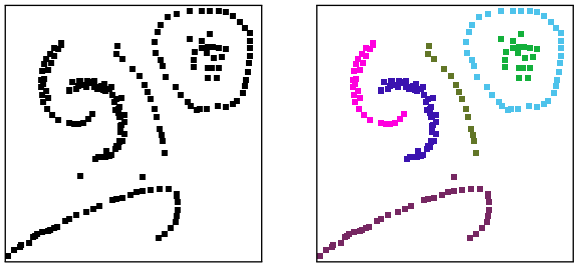

Figure 4: Illustration of the advantages of clustering with the DBSCAN method which is the basis for the Minima Clustering we present. DBSCAN can correctly identify and separate curved clusters where the convex hull is overlapping, as seen with the blue and pink cluster. It also correctly identifies and separate clusters within clusters as seen with the green and light blue clusters.

4.2.1. Minima Clustering

To cluster the minima we use an approach based on Density-Based Spatial Clustering of Applications with Noise (DBSCAN), a density-based clustering method introduced by Ester et al. [EKSX96]. DBSCAN utilizes a region growing technique, starting at a single point it finds all points within a certain radius and adds them to the cluster. The growing technique is iteratively applied to all new points in the cluster until it has found all points to be included. Thanks to the growing scheme used by DBSCAN it can accurately identify and separate clusters within clusters and non-convex clusters with overlapping convex hull, as illustrated in Figure 4. To cope with noisy data DBSCAN marks a point as noise if it has less than N points within the given radius, points marked as noise are not included in any cluster. The original version of DBSCAN uses the Euclidean distance. In the case of the coherence map that might result in clusters falsely joined across a ridge. An example of regions where this can be a problem can be seen in the zoomed region in Figure 5. To address this we use a modification of the Euclidean distance metric, sampling the FTLE values between the two minima. Then, two minima are only consider as part of the same cluster if the maximum FTLE value in-between them falls below the coherence threshold.

4.2.2. Context Aware Minima Expansion

After clustering of the minima they are expanded to regions of coherent flow. The minima are used as seeds, starting with the smallest minima. The regions are then grown to neighboring pixels using their 8-neighborhood. The neighboring pixel is added if the difference in intensities compared to current pixel is less then a certain ΔI

and if the intensity of the neighboring pixel is less than the coherence threshold. This will grow the sparse regions from the minima clustering into a dense cluster of both regular pixels and local minima, only the local minima that is not yet in a cluster is used as seed for new clusters. This is iteratively done until all minima are in a cluster.

4.3. Coherent flow feature representation

For the visualization of the coherent flow regions, we provide a set of methods to represent clusters visually, ranging from cluster representatives to full cluster visualization. The user can easily toggle between these modes by clicking on the cluster with the mouse. The first method to represent a cluster is a single pathline representative. Since in general the shapes of the clustered regions are not convex and can be quite elongated or bent a simple average computation can lead to positions outside the cluster. Instead we need a robust strategy to pick a cluster member that is both inside the region and represents the flow in a good way. We experimented with various options for the representative definition which all lead to similar results as they represent the same coherent region. Among others we considered the following options: Cluster member that is closest to the average. This ensures that the selected point is inside the current region. Though, in the case where the average point is outside of the region it will most likely be on the boundary of the region. Cluster member with the highest coherence value. This ensures that the selected lines exhibits a high similarity to its neighbors. From a perceptual point of view it is also an option to chose the longest pathline of the cluster. Depending on the size of the cluster it might also be desirable to inspect the internal structure of the entire cluster which is not visible from one representative, e.g. a twisting behavior. Therefore we also support to show the entire cluster with user determined density by randomly sampling the cluster region. Since one or more clusters may be hidden completely a visualization of various combinations of full clusters and representatives is possible as can be seen in Figures 6 and 10.

The regions extracted with the proposed method can, per definition, only visualize the flow in coherent regions, therefore we add the option to display all or a random sampled subset of the pathlines that are not part of any cluster, two examples of this can been found in Figure 6e and 2. By allowing to alternate between showing the coherent flow and the non-coherent flow we support visualization of all flow that originates from the slice.

Lastly, to support size comparison of the coherent regions we display a pie chart in which each cluster is present and the area of each slice can either represent the size of each cluster in terms of cluster area or the volume of fluid that passes through the plane at the given point in time by integrating the velocities. On demand the pie chart also takes the non-coherent regions into consideration.

4.4. Interactive exploration

While the automatic clustering approach and its representation described above is very useful to locate and represent coherent flow it is also important to provide possibilities to interact with the data, analyzing individual clusters as well as the non coherent regions. The basic interface for interaction consists of three parts which are linked together: the coherence map, the cluster pie chart and the three dimensional rendering. The user can add, move and remove representatives of various colors directly on the coherence map and see the resulting visualization in real-time in a linked view. We also support live preview of not yet added points by seeding new pathlines under the mouse cursor when hovering the coherence map. These tools allow the user to explore the flow in less coherent regions with high FTLE values and see of how marginal movements of the seeding position will affect the trajectories. This leads not only to a better representation and understanding of the flow, but also a better understanding of concepts of the coherence map and a greater trust in the automatic approaches presented. The cluster pie chart can also be used to select or deselect individual clusters. For the tree dimensional rendering various options are provided between the user can switch, see Section 4.3.

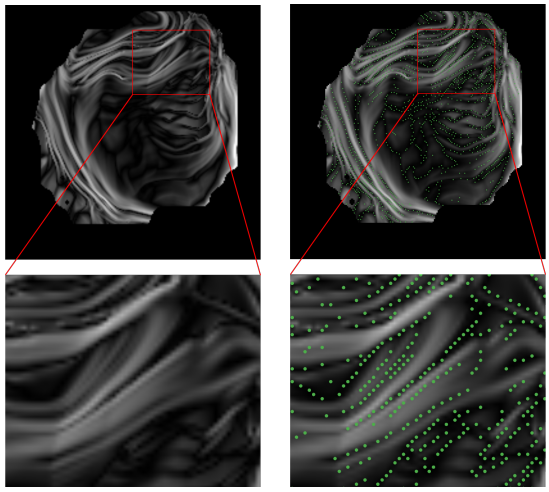

(a) (b)

Figure 5: The coherence map generated from placing the a 2D slice through the beginning of the aorta. (a) shows the coherence map and (b) shows the map together with the local minima. In the magnified area we can clearly there are plenty of minima along apparent valleys and ridges that need to be separated during clustering.

5. Results

The concepts presented in this paper has been implemented into Inviwo, a data-flow development environment for scientific visualization [SSK*15]. The examples shown in this paper was produced using a computer with a 3.5 GHz Intel i7-4770K processor, 32 GB RAM and a NVIDIA GeForce GTX 660 graphics card. We have applied the algorithm to two blood flow datasets. The first dataset is a 4D flow MRI scan of a heart with the chambers and vessels of the heart segmented [BPE*15] and the second one is a blood flow simulation of a brain aneurysm. While both the heart dataset and the aneurysm dataset represent blood flow, the heart dataset is acquired by measurements and therefore has a lower signal to noise ratio then the aneurysm dataset which is generated from computational fluid simulations. In the following sections we describe the data in more detail and show that our techniques works well on data

with more or less noise in it. For all examples in the paper we use 4th order Runge-Kutta for pathline and streamline integration.

5.1. Cardiac Blood Flow from 4D flow MRI

The first dataset is a measurement using a 4D flow MRI sequence containing the flow of a full heart cycle of a healthy patient. The sequence consists of 40 timesteps, each stored as a volume with $112 \times 112 \times 48$ voxels. The dataset has been segmented into masks defining each of the four chambers and major vessels of the heart [BPE*15]. The slice for the FTLE calculation is placed in the ascending aorta as a cross section oriented normal to the mean flow. The pathlines for the flow map are seeded on a 200×200 grid. For all examples with the 4D flow MRI dataset it takes about 8.5 seconds to create the coherence map and the radius parameter for the DBSCAN was set to 9 pixels and the coherence threshold were set to 4.5. The first timestep selected is $t = 0$ and the pathlines are integrated for a duration of 0.4 seconds. This corresponds roughly to the start and duration of the ventricular systole, the phase of the heart cycle where the ventricle contracts and blood is pushed out of the left ventricle resulting in high velocities in the aorta.

The coherence map (Figure 7a) has values ranging from 0.001 to 18.692 and contains 1680 local minima. The Automatic Coherent Region Extraction (Sec 4.2) locates 18 prominent clusters ($N > 10$, where N is the number of pathlines in the cluster). There is one large region, spanning from the center of the map to the bottom right corner, representing the main flow through the aortic arc and into the descending aorta. Around the large cluster we have a set of smaller clusters representing blood flow either towards the arteries or the descending aorta. Figure 1a displays the results showing the seven most prominent cluster ($N > 100$).

To explore the changes of the flow patterns over the heart cycle we use three timesteps for the FTLE calculation, shown in Figure 1. A first observation is that throughout the heart cycle the amount of inflow in the aorta varies strongly. The integration time for all start times is the same, but the pathlines for $t = 0.6$ are much shorter than for $t = 0$ and $t = 0.3$, Figure 1c. Timestep $t = 0.6$ captures the behavior of the heart cycle during the diastole, a phase of the heart cycle where the flow in the aorta is at a minimum, which is clearly visible when comparing it to the other timesteps. A more interesting timestep is $t = 0.3$, Figure 1b, which captures the end of the ventricular systole and the beginning of ventricular diastole. This includes the closing of the valve between the left ventricle and the aorta which decrease the flow through the aorta to a minimum and introducing some backflow. The flow of this timestep is further explored in Figure 6 in which we have selected various clusters such that we show the underlaying pathlines for each of the clusters instead of the representatives.

5.2. Aneurysm Blood Flow from CFD Simulation

The second dataset is a simulation of blood flowing through an cerebral saccular aneurysm [GSS*14]. The data is the result of a computational fluid dynamics (CFD) simulation on a unstructured grid. The data set provides the accurate geometry of the simulation and velocity values associated to the tetrahedra. For the computation of the coherence map the data has been resampled onto a structured grid of size 330x280x280. This size was selected since it aligns with the shortest edge of all tetrahedra in the tetrahedral mesh. The data contains only is not time-resolved, so streamlines are used instead of pathlines.

The slice for the FTLE calculation is placed such, that it intersects the vessel that supplies the aneurysm with blood. Streamlines are seeded on the slice with a resolution of 150×150 and traced for a total of 500 steps, each with a step length of 0.01. For all examples with the aneurysm dataset the radius parameter for the DBSCAN was set to 22 pixels and the coherence threshold were set to 1.2. The resulting coherence map (Figure 2a) was constructed in 4.8 seconds and consists of 966 minima (Figure 2b) and has a value range between 0.015 and 2.576. Automatic Coherent Region Extraction locates 18 prominent clusters ($N > 10$). Figures 2(g-i,c-d) display the 5 most prominent of these. In Figure 10(f-j) the clusters are further explored by showing only the streamlines within selected cluster.

In the histograms of the FTLE values in Figure 8 we can see that the coherency map of this dataset contains a higher ratio of large FTLE values compared the 4D flow MRI dataset. This is expected due to the fact that blood entering the aneurysm has a high velocity and travels fairly straight until it hits the wall, since the flow hits the wall at a rather large angle the flow is diverted out in all directions resulting in a high present of non-coherent flow behavior. This can clearly be seen in Figure 10f and 10g where the two most prominent cluster are first traveling on similar trajectories and when they reach the wall they divert in two different directions. This results in large regions which is not covered by any cluster and it is not possible to find good representatives here. The interactive exploration described in section 4.4 serves as a good tool to explore the flow in these areas. This is demonstrated in Figure 9 in which we have manually seeded 4 stream ribbons in close proximity of each other in a region where the coherence map is indicating low coherence. The resulting stream ribbons initially follow the same flow, but as soon they reach the wall of the aneurysm they diverge and end up having very different trajectories. This example clearly demonstrates the advantage or method of displaying the coherence map together with the coherent features in comparison to other streamlines clustering methods. Our method provides an impression of the dominant features in the flow however also communicates which parts of the flow cannot be capture by any clustering and can be further explored by interactively placing seeds in the coherence map.

6. Conclusion

We have presented a semi-automatic method to explore time-dependent flow data with a clearly defined inflow and outflow area. It uses the concept of coherent structures and FTLE as a similarity measure for pathlines. The central element of our approach is a 2D FTLE coherence map summarizing the flow volume by exploring the pathlines entering the volume. The coherence map guides the automatic coherent feature generation capturing the dominant trends in the flow. These trends can be visualized as dominant flow cluster or as representative pathlines. However, most importantly it also provides a means to understand the relevance of the automatically extracted features and detect regions that are not well represented by the clusters. In this way the coherent feature extraction

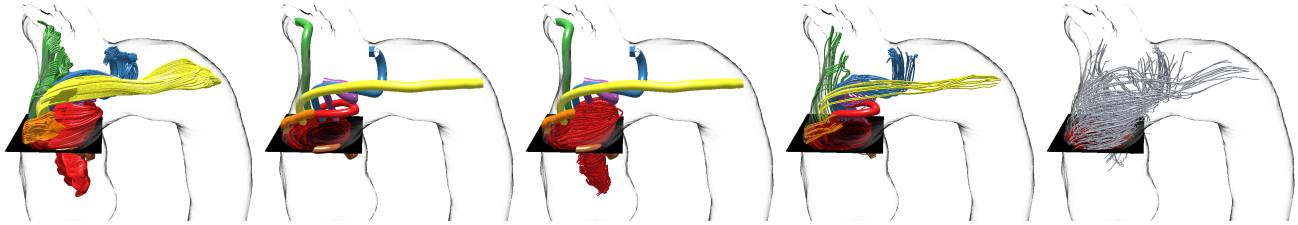

(a) (b) (c) (d) (e)

Figure 6: Results from the 4D flow MRI dataset where pathlines are seeded in the ascending aorta at $t = 0.3$. (a) shows all pathlines in the seven most prominent regions, (b) shows their representatives. In (c) we show all pathlines of the red cluster while only the representatives of the other clusters are selected. In (d) we show the reversed selection, the representative for the red cluster and the pathlines of the other clusters. In (e) we see the pathlines originating from the remaining regions which are not part of one of the dominant clusters. A closer inspection of the coherence map and the size of the located clusters can be found in Figure 7.

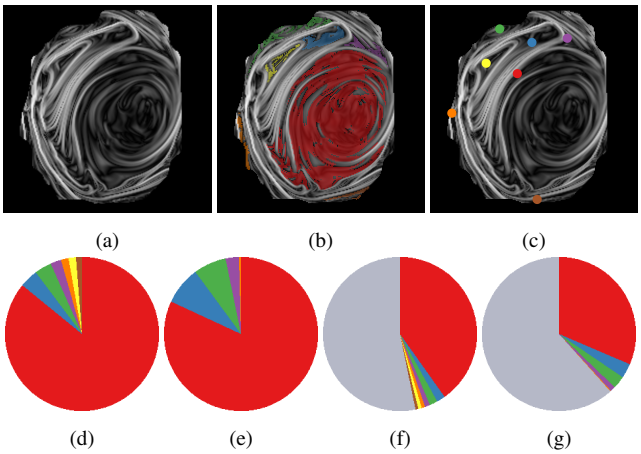

(a) (b) (c) (d) (e) (f) (g)

Figure 7: Coherence map of the 4D flow MRI dataset at $t = 0.3$ (a) the map, (b) the seven most prominent clusters (c) the seeding position of their representatives. The respective flow clusters are displayed in Figure 6. (d-e) show the relative size of the clusters, (d, f) by area measured by the number of included pathlines and (e, g) by the volume passing through the slice at the starting timestep. The gray regions in (f) and (g) represent the portion of the pathlines that originates from regions not included in the selected clusters.

process becomes transparent to the user and is not just a black box generating pretty images. The coherence map can also be used as intuitive interface for a further interactive exploration of the flow. The few parameters involved in the extraction process can be interactively adapted and will mainly influence the number of displayed clusters and their level of detail. Our results demonstrate clearly that it is often not possible to capture the entire dynamics of the flow fields using some clusters and there are always regions which need a closer inspection and provides a good alternative to traditional clustering methods. The tool provides a good combination of automatic feature extraction and possibilities to investigate the flow manually. This can serve as a valuable basis for the understanding of typical blood flow characteristics and the development hypothesis that can be used in future clinical studies.

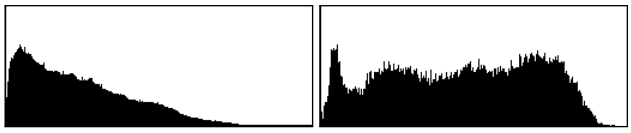

(a) 4D flow MRI heart dataset at t=0 (b) CFD Aneurysm dataset

Figure 8: Histogram of the the coherency maps. Values to the left represent high coherency (low FTLE values) and values to the right represent low coherency. The axis are scaled to fit the data of the given dataset.

References

[AH11] ANGELELLI P., HAUSER H.: Straightening tubular flow for side-by-side visualization. *IEEE Trans. Vis. Comput. Graph. 17*, 12 (2011), 2063–2070. 4

[BC13] BYRNE G., CEBRAL J.: Vortex dynamics in cerebral aneurysms. *arXiv:1309.7875v1* (2013). 4

[BGT12] BARAKAT S., GARTH C., TRICOCHE X.: Interactive computation and rendering of finite-time lyapunov exponent fields. *IEEE Trans. Vis. Comput. Graph. 18*, 8 (2012), 1368–1380. 3

[BMGS13] BORN S., MARKL M., GUTBERLET M., SCHEUERMANN G.: Illustrative visualization of cardiac and aortic blood flow from 4d mri data. In *IEEE Pacific Visualization Symposium* (2013). 3

[BPE*15] BUSTAMANTE M., PETERSSON S., ERIKSSON J., ALEHAGEN U., DYVERFELDT P., CARLHÄLL C.-J., EBBERS T.: Atlas-based analysis of 4d flow cmr: Automated vessel segmentation and flow quantification. *J Cardiovasc Magn Reson 17* (2015). 6, 7

[BPM*13] BORN S., PFEIFLE M., MARKL M., GUTBERLET M., SCHEUERMANN G.: Visual analysis of cardiac 4D MRI blood flow using line predicates. *IEEE Trans. Vis. Comput. Graph. 19*, 6 (2013), 900–12. 2, 3

[CBB*14] CARNECKY R., BRUNNER T., BORN S., JÜRGEN WASER, HEINE C., PEIKERT R.: Vortex detection in 4d mri data: Using the proper orthogonal decomposition for improved noise-robustness. In *Short Paper Eurovis'14* (2014), pp. 127–131. 3

[Cha10] *Chaos: An Interdisciplinary Journal of Nonlinear Science (Special issue on Lagrangian coherent structures)*, vol. 20. American Institute of Physics (AIP), 2010. 3

[CYY*11] CHEN C.-K., YAN S., YU H., MAX N., MASAHIRO K.-L.: An illustrative visualization framework for 3d vector fields. *Computer Graphics Forum 30*, 7 (2011), 1941–1951. 2

[ECE*10] ERIKSSON J., CARHÄLL C., ENGVALL P., BOGER A. F.,

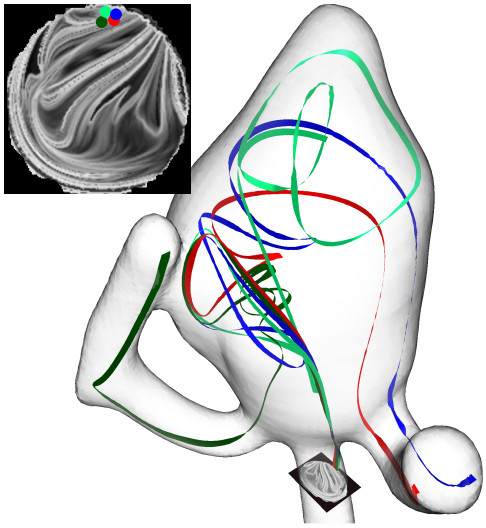

Figure 9: Four streamlines have manually been selected in a close neighborhood exhibiting low coherency values. The resulting trajectories clearly diverge from each other, an indication of a region of high turbulence. This behavior cannot be captured by any clustering algorithm.

EBBERS T.: Semi-automatic quantification of 4d left ventricular blood flow. *Journal of Cardiovascular Magnetic Resonance* (2010). 3

[EKSX96] ESTER M., KRIEGEL H.-P., SANDER J., XU X.: A density-based algorithm for discovering clusters in large spatial databases with noise. In *Proceeding of Kdd* (1996), vol. 96, pp. 226–231. 5

[FSP12] FUCHS R., SCHINDLER B., PEIKERT R.: Scale-space approaches to ftle ridges. In *Topological Methods in Data Analysis and Visualization. Theory, Algorithms, and Applications*. Springer, 2012, pp. 283–296. 3

[GBWT11] GÜNTHER T., BÜRGER K., WESTERMANN R., THEISEL H.: A view-dependent and inter-frame coherent visualization of integral lines using screen contribution. In *Proceedings of Vision, Modeling, and Visualization* (2011). 2

[GGTH07] GARTH C., GERHARDT F., TRICOCHE X., HAGEN H.: Efficient computation and visualization of coherent structures in fluid flow applications. *IEEE Trans. Vis. Comput. Graph. 13*, 6 (2007), 1464–1471. 3, 5

[GLvP*12] GASTEIGER R., LEHMANN D. J., VAN PELT R., JANIGA G., BEUING O., VILANOVA A., THEISEL H., PREIM B.: Automatic detection and visualization of qualitative hemodynamic characteristics in cerebral aneurysms. *IEEE Trans. Vis. Comput. Graph. 18*, 12 (2012), 2178–2187. 4

[GNBP11] GASTEIGER R., NEUGEBAUER M., BEUING O., PREIM B.: The flowlens: A focus-and-context visualization approach for exploration of blood flow in cerebral aneurysms. *IEEE Trans. Vis. Comput. Graph. 17*, 12 (2011), 2183–2192. 3

[GNKP10] GASTEIGER R., NEUGEBAUER M., KUBISCH C., PREIM B.: Adapted surface visualization of cerebral aneurysms with embedded blood flow information. In *Eurographics Workshop on Visual Computing for Biology and Medicine* (2010). 3

[GRT13] GÜNTHER T., RÖSSL C., THEISEL H.: Opacity optimization for 3d line fields. *ACM Transactions on Graphics 32*, 4 (2013), 120:1–120:8. 2

[GSS*14] GOUBERGRITS L., SPULER A., SCHALLER J., WIEGMANN N., BERTHE A., HEGE H.-C., AFFELD K., KERTZSCHER U.: In vitro study of hemodynamic treatment improvement: Hunterian ligation of a fenestrated basilar artery aneurysm after coiling. *The International Journal of Artificial Organs 37*, 4 (2014), 325–335. 7

[GTS*04] GARTH C., TRICOCHE X., SALZBRUNN T., BOBACH T., SCHEUERMANN G.: Surface techniques for vortex visualization. In *VisSym '04: Proceedings of the Symposium on Data Visualization 2004* (2004), pp. 155–164. 3

[Hal01] HALLER G.: Distinguished material surfaces and coherent structures in three-dimensional fluid flows. *Phys. D 149*, 4 (2001), 248–277. 2, 3, 4

[Hus83] HUSSAIN A. K. M. F.: Coherent structure – reality and myth. *Physics of Fluids 26*, 10 (1983), 2816–2850. 2, 3

[KBvP*15] KÖHLER B., BORN S., VAN PELT R. F. P., PREIM U., PREIM B.: A survey of cardiac 4d pc-mri data processing. In *Proceedings of the Eurographics Workshop on Visual Computing for Biology and Medicine* (2015), pp. 139–148. 3

[KGG*12] KRISHNAN H., GARTH C., GÜHRING J., GÜLSÜN M. A., GREISER A., JOY K. I.: Analysis of time-dependent flow-sensitive pc-mri data. *IEEE Trans. Vis. Comput. Graph. 18*, 6 (2012), 966–977. 3

[KGP*13] KÖHLER B., GASTEIGER R., PREIM U., THEISEL H., GUTBERLET M., PREIM B.: Semi-automatic vortex extraction in 4d pc-mri cardiac blood flow data using line predicates. *IEEE Trans. Vis. Comput. Graph. 19*, 12 (2013), 2773–2782. 2, 4

[KHH12] KASTEN J., HOTZ I., HEGE H.-C.: On the elusive concept of lagrangian coherent structures. In *Topological Methods in Data Analysis and Visualization II. Theory, Algorithms, and Applications*, Mathematics and Visualization. Springer, 2012, pp. 207–220. 3

[KPH*09] KASTEN J., PETZ C., HOTZ I., NOACK B., HEGE H.-C.: Localized Finite-time Lyapunov Exponent for Unsteady Flow Analysis. In *Proceedings of Vision, Modeling, and Visualization (VMV'09)* (2009), vol. 1, pp. 265–274. 3

[KRaHCH*16] KASTEN J., REININGHAUS J., ADN HANS-CHRISTIAN HEGE I. H., NOACK B. R., DAVILLER G., MORZYNSKI M.: Acceleration feature points of unsteady shear flows. *Archives of Mechanics 68*, 1 (2016), 29. 3

[Lan13] LANTZ J.: *On Aortic Blood Flow Simulations, Scale-Resolved Image-Based CFD*. PhD thesis, Linköping University, devision of applied thermodynamics and fluid mechanics, 2013. 3

[LCL*13] LU K., CHAUDHURI A., LEE T.-Y., SHEN H.-W., WONG P. C.: Exploring Vector Fields with Distribution-based Streamline Analysis. In *IEEE Pacific Visualization Symposium* (2013). 2

[LM10] LIPINSKI D., MOHSENI K.: A ridge tracking algorithm and error estimate for efficient computation of lagrangian coherent structures. *CHAOS 20*, 1 (2010), 017504. 3

[LMSC11] LEE T.-Y., MISHCHENKO O., SHEN H.-W., CRAWFIS R.: View point evaluation and streamline filtering for flow visualization. In *IEEE Pacific Visualization Symposium* (2011), pp. 83–90. 2

[MAD05] MEBARKI A., ALLIEZ P., DEVILLERS O.: Farthest point seeding for efficient placement of streamlines. In *Proceedings of IEEE Visualization 2005* (2005), pp. 479–486. 2

[MCHM10] MARCHESIN S., CHEN C.-K., HO C., MA K.-L.: View-dependent streamlines for 3d vector fields. *IEEE Trans. Vis. Comput. Graph. 16*, 6 (2010), 1578–1586. 2

[MJL*13] MCLOUGHLIN T., JONES M. W., LARAMEE R. S., MALKI R., MASTERS I., HANSEN C. D.: Similarity measures for enhancing interactive streamline seeding. *IEEE Transaction on Visualization and Computer Graphics 19*, 8 (2013), 1342–53. 2

[MKE11] MARKL M., KILNER P. J., EBBERS. T.: Comprehensive 4d velocity mapping of the heart and great vessels by cardiovascular magnetic resonance. *Journal of Cardiovascular Magnetic Resonance (BioMed Central) 13*, 1 (2011), 1. 3

[MKP*16] MEUSCHKE M., KÖHLER B., PREIM U., PREIM B., LAWONN K.: Semi-automatic vortex flow classification in 4d pc-mri data of the aorta. *Computer Graphics Forum (EuroVis'16) 35*, 3 (2016). 4

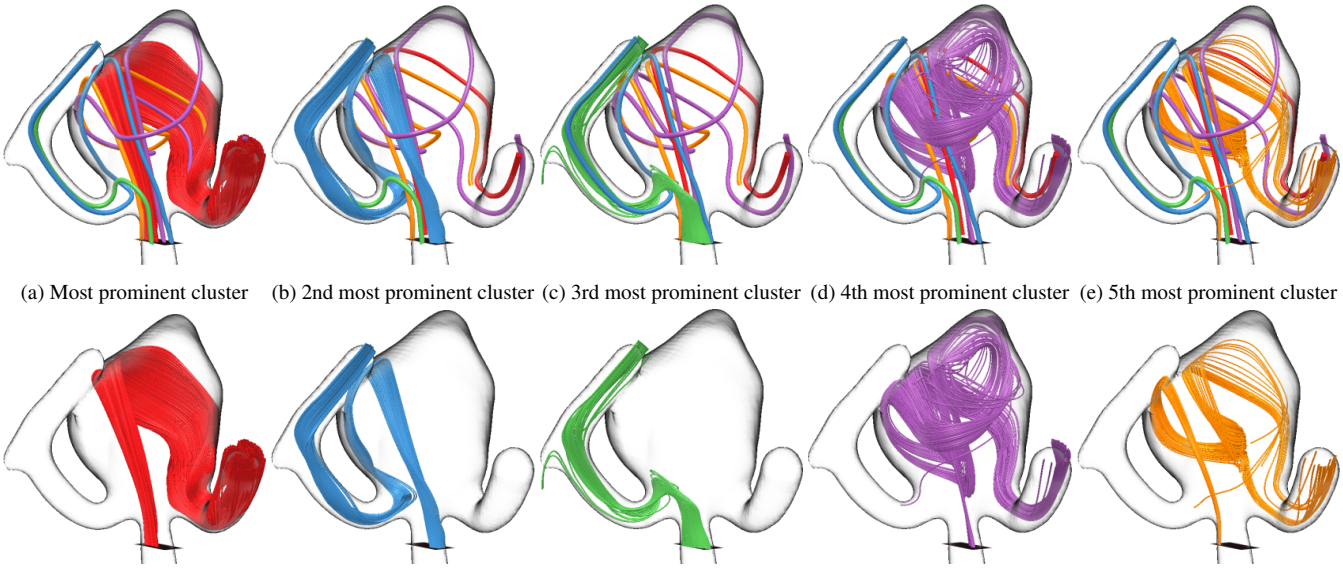

(a) Most prominent cluster (b) 2nd most prominent cluster (c) 3rd most prominent cluster (d) 4th most prominent cluster (e) 5th most prominent cluster

(f) Most prominent cluster (g) 2nd most prominent cluster (h) 3rd most prominent cluster (i) 4th most prominent cluster (j) 5th most prominent cluster

Figure 10: Depiction of the underlaying flow structures of the five most prominent cluster found in the aneurysm dataset. On the top row we see each cluster selected together with the representatives for the other clusters and on the bottom row, we have selected the same clusters, but showing only the selected cluster.

[MVvW05] MOBERTS B., VILANOV A., VAN WIJK J.: Evaluation of fiber clustering methods for diffusion tensor imaging. *Proceedings of IEEE Visualization Conference* (2005), 65–72. 2

[OJCJP16] OELTZE-JAFRA S., CEBRAL J. R., JANIGA G., PREIM B.: Cluster analysis of vortical flow in simulations of cerebral aneurysm hemodynamics. *IEEE Trans. Vis. Comput. Graph. 22*, 1 (2016), 757–766. 2, 4

[OLTP12] OELTZE S., LEHMANN D. J., THEISEL H., PREIM B.: *Evaluation of Streamline Clustering Techniques for Blood Flow Data*. Tech. rep., Otto-von-Guericke-Universität Magdeburg, 2012. 2

[POS*11] PAGOT C., OSMARI D., SADLO F., WEISKOPF D., ERTL T., COMBA J.: Efficient parallel vectors feature extraction from higher-order data. *Computer Graphics Forum 30*, 3 (2011), 751–760. 3

[PPSS14] PEIKERT R., POBITZER A., SADLO F., SCHINDLER B.: A comparison of finite-time and finite-size lyapunov exponents. In *Topological Methods in Data Analysis and Visualization III. Theory, Algorithms, and Applications*, Bremer P.-T., Hotz I., Pascucci V., Peikert R., (Eds.), Mathematics and Visualization. Springer, 2014. 3

[RPH*09] ROSANWO O., PETZ C., HOTZ I., PROHASKA S., HEGE H.-C.: Dual streamline seeding. In *IEEE Pacific Visualization Symposium* (2009), pp. 9–16. 2

[SAG10] SHADDEN S. C., ASTORINO M., GERBEAU J.-F.: Computational analysis of an aortic valve jet with lagrangian coherent structures. *CHAOS 20*, 1 (2010), 017512. 3

[SCTC12] SANDERSON A., CHEN G., TRICOCHE X., COHEN E.: Understanding quasi-periodic fieldlines and their topology in toroidal magnetic fields. In *Topological Methods in Data Analysis and Visualization II. Theory, Algorithms, and Applications*, Mathematics and Visualization. Springer, 2012, pp. 125–140. 3

[SGSM08] SALZBRUNN T., GARTH C., SCHEUERMANN G., MEYER J.: Pathline predicates and unsteady flow structures. *The Visual Computer 24*, 12 (2008), 1039–1051. 2

[SLM05] SHADDEN S. C., LEKIEN F., MARSDEN J. E.: Definition and properties of lagrangian coherent structures from finite-time lyapunov exponents in two-dimensional aperiodic flows. *Physica D 212(3-4)* (2005), 271–304. 2, 3

[SP07] SADLO F., PEIKERT R.: Efficient Visualization of Lagrangian Coherent Structures by Filtered AMR Ridge Extraction. *IEEE Trans. Vis. Comput. Graph. 13*, 6 (2007), 1456–1463. 3

[SPK*12] SENGUPTA P. P., PEDRIZZETTI G., KILNER P. J., KHERADVAR A., EBBERS T., TONTI G., FRASER A. G., NARULA J.: Emerging trends in cv flow visualization - state of the art. *JACC Journal on Cardiovascular Imaging 5*, 3 (2012). 3

[SSK*15] SUNDÉN E., STENETEG P., KOTTRAVEL S., JÖNSSON D., ENGLUND R., FALK M., ROPINSKI T.: Inviwo—An Extensible, Multi-Purpose Visualization Framework. Poster at IEEE Vis, 2015. 6

[ST08] SHADDEN S. C., TAYLOR C. A.: Characterization of coherent structures in the cardiovascular system. *Annals of Biomedical Engineering 36*, 7 (2008), 1152–1162. 3

[TSH01] TRICOCHE X., SCHEUERMANN G., HAGEN H.: Continuous Topology Simplification of Planar Vector Fields. In *Proceedings of the conference on Visualization '01* (2001), pp. 159–166. 3

[vPBB*11] VAN PELT R., BESCOS J. O., BREEUWER M., CLOUGH R. E., GRÖLLER E., ROMENY B. H., VILANOVA A.: Interactive virtual probing of 4d mri blood-flow. *IEEE Trans. Vis. Comput. Graph. 17*, 12 (ec 2011), 2153–2162. 4

[vPFCV14] VAN PELT R., FUSTER A., CLAASSEN1 G., VILANOVA A.: Characterization of blood-flow patterns from phase-contrast mri velocity fields. In *ShortPaper EuroVis'14* (2014). 4

[vPJtHRV12] VAN PELT R. F. P., JACOBS S., TER HAAR ROME B., VILANOVA A.: Visualization of 4d blood-flow fields by spatiotemporal hierarchical clustering. *Computer Graphics Forum 31* (2012), 1065–1074. 4

[YWSC12] YU H., WANG C., SHENE C.-K., CHEN J. H.: Hierarchical streamline bundles. *IEEE Trans. Vis. Comput. Graph. 18*, 8 (2012), 1353–1367. 2